Hindawi
Journal of Renewable Energy
Volume 2023, Article ID 8836777, 15 pages
https://doi.org/10.1155/2023/8836777

Research Article

Year-Round Experimental Analysis of the Productivity of Vapour-Based Multistage Solar Still: A Developmental Study

Mfanafuthi Mthandeni Mkhize and Velaphi Msomi

Cape Peninsula University of Technology, Faculty of Engineering and the Built Environment, Mechanical Engineering Department, P.O. Box 1906, Bellville 7535, South Africa

Correspondence should be addressed to Mfanafuthi Mthandeni Mkhize; sggamkhize@gmail.com

Received 17 December 2022; Revised 5 March 2023; Accepted 10 March 2023; Published 28 March 2023

Academic Editor: Jing Shi

The standalone vapour-based multistage solar still with stacked stages (MSS-SS) belongs to a pool of widely studied small-scale water desalination devices through solar thermal energy. This work contributes to the body of knowledge by presenting a system with new configurations. There is a need to develop small-scale systems to be reliable devices for freshwater provision, as brackish water is available for processing. The experimental study was conducted in a field under actual weather conditions, with the data logged and analysed to study the systems' behaviour under varying meteorological conditions. A maximum distillate yield of 7790 ml, corresponded to a maximum daily average solar radiation at high range. There was a 21.8% decrease to 6090 ml at moderate daily average range and a further decline of 80.5% to 1190 ml in the low daily average range, representing a significant drop in the distillate yield caused by the insufficient heat collection at low range. The high, moderate, and low ranges corresponded to summer, spring and autumn, and winter, respectively. The lower values of the moderate range were the most optimum operationally. The impulsive modes were ideal for high rates of the heat inputs, while the continuous were for low rates. The assumption of a continuous mode and a further increase in the rate of thermal energy input caused thermal damage necessitating the augmentation of the thermal energy storage (TES) device due to a larger collector-to-basin area (CBA) ratio. The distillate yield trends from the stages were dynamic and were the inverse of the stage temperature, which was dictated by the mode and rate of the thermal energy input. These trends were such that stage 5 > 3 > 2 > 1 > 4 at moderate to high ranges and changed a low range. The summer season enhanced the cumulative saline water (SW) preheating and heat recovery to 66.8°C. The economic analysis found that at its most productive level, the cost of producing water per litre (CPL) from the vapour-based MSS-SS was *R* 4.05. The small-scale water purification systems are helpful, especially in remote areas.

1. Introduction

Due to increasing demands from different sectors, there are increasing opportunities for decentralised water desalination. Rapid industrialisation, the farming sector, urbanisation, and the growing population need access to clean water. Water desalination is possible from readily available water sources such as rivers, lakes, boreholes, surface rainwater, and seawater. Decentralised desalination methods such as solar stills are advantageous for remote and isolated areas such as rural areas not connected to piped water supplies. Solar stills, which can also be portable, with various configurations and types, are ideal for any freshwater scarcity-stricken regions [1, 2]. Depending on its design, solar stills can operate anywhere so long as there is enough solar radiation as its primary energy source. The small-scale solar stills desalt water based on the greenhouse effect using solar energy powered by clean and environmentally friendly sources [3]. However, the downside of solar stills is their low productivity and efficiency. Many methods have been used to improve the solar still's performance, optimise its operation, and enhance the heat transfer processes, such as integrating solar stills with the phase-changing material (PCM), fins, nanoparticle/nanofluids, and solar collectors, incorporating heat exchanger to enhance the distillate yield and productivity [4–6].

In the study by El-Sebaii and El-Naggar [7], the average and maximum values of global solar radiation measured on the horizontal surface were 719.72 and 990.0 W/m^2, respectively, in summer. The corresponding ambient temperature values were 31.5 and 35°C, respectively. In winter, these values were 293.81 and 599.0 W/m^2, respectively, while the ambient temperature values were 17.98°C and 19.0°C, respectively. The distillate yield was the function of prevailing solar radiation; that is, the productivities of the finned basin liner still (FBLS) and the conventional still (CS) were minimum in the winter and maximum in the summer. For the FBLS, the productivity fluctuated from 2.966 kg/m^2 day to 6.764 kg/m^2 day from winter to summer, respectively. In contrast, the CS varied from 2.397 k/m^2·day to 5.11 kg/m^2·day from winter to summer. The corresponding efficiency values were 50.27% and 57.69% in winter and summer for the FBLS, respectively. For the CS, these efficiency values were 40.7% and 44.88% in the winter and summer seasons, respectively. Finally, the cost of distillate production per litre was the cheapest for the FBLS at 0.2 LE (Egyptian pound).

A comparative study by Srivastava and Agrawal [8] between the finned solar still and the CS reported that both stills were most productive in summer. The finned solar still maintained enhanced daily cumulative distillate yields compared to the CS in both winter and summer. Moreover, the winter season experienced a more significant percentage increase in the daily cumulative distillate yield between the two stills. Maximum distillate yields of 7.5 kg/m^2 and 6.5 k/m^2 for the finned solar still and the CS were achieved in the summer, respectively. Furthermore, an increase in the SW depth in the still's basin inversely affected its productivity.

Muftah et al. [9] conducted a performance evaluation study on a basin-type stepped solar still with the low thermal inertia of water mass in which modified and unmodified solar stills were compared. The solar still coupled with the internal and external reflectors was reported to receive a maximum solar incidence of 1450 W/m^2 with the ambient air temperature reaching the highs of approximately 35°C to 36°C at noon in Malaysia. Furthermore, SW in the modified and unmodified solar stills attained the maximum temperatures of 68.1°C and 63.4°C, respectively. Increasing wind velocity had notable effects on the productivity of the stills as it reduced the condensing cover temperature, which enhanced the condensation process due to the more considerable temperature difference between the SW and the condensing glass cover. A 29% increase in the daily cumulative distillate yield was achieved from the modified solar still over the unmodified one; their daily cumulative distillate yields were 8.9 kg/m^2 and 6.9 kg/m^2, respectively. Lastly, the modified and unmodified solar stills efficiencies were 60.2% and 52.3%, respectively.

Kumar et al. [10] reported that an active solar distillation system was most productive during the months of April, May, and October for the climate conditions in Delhi, India. Furthermore, an increase in the SW depth inversely affected the annual productivity of the still. The optimum condensing glass inclination and the flat plate solar collector (FPSC) were 15° and 20° from the horizontal surface, respectively. In a review study by Elsheikh et al. [11], there has been a surge of recent studies investigating a thin water film layer for steam generation (SG). While the thermal efficiency of solar stills with the bulk bodies of water ranged between 30 and 45%, the SG devices can reach as high as 95% thermal efficiency. The study also suggests that the materials such as wood, which is readily available and of low-cost, can be used to enhance the thermal efficiency of these devices. An optimisation study was reported by Kumar et al. [12] with maximum solar radiation and ambient air temperature of 955.56 W/m^2 and 36.1°C, respectively, in March for a location in Chennai, India. In December, the corresponding values were 705.56 W/m^2 and 27.9°C, respectively. The study reported various findings, some of which were an optimum number of the stacked stages was four (4), stage gap was 100 mm, parallel connected FPSC achieved the highest SW temperature output, SW flow rate was optimum at 55 kg/m^2 day, decreased wind velocity reduced heat losses from the FPSC, and optimum distillate yield of 28.044 kg/m^2 day at atmospheric pressure. Lastly, it was reported that the upper stages tended to be more productive than the lower stages due to the cumulative SW preheating effects through latent condensation heat from the lower stages. Furthermore, solar stills optimisation can be enhanced by incorporating cutting-edge and modern artificial intelligence (AI) technology. It has been shown elsewhere that using multilayer perceptron (MLP) to predict the solar still's thermal efficiency has a relative error of approximately 10%. Furthermore, using artificial intelligence accurately predicts thermal efficiency and the overall performance of the system. [13–15].

Feilizadeh et al. [16] reported on an experimental investigation of multistage solar still with four stacked trays. The basin (bottom-most stage) was filled with 20 kg of SW, while the rest of the stages with 14 kg each. The number of FPSCs connected in series varied with season during the study of the effect of the CBA ratio. The CBA ratios were 3.45 (1 FPSC), 6.90 (2 FPSC), and 10.35 (3 FPSC). Ethylene glycol was employed as a heat transfer fluid (HTF) to supply heat in the basin (bottom-most stage).

Furthermore, the sequential heat transfer between the stages was such that the lower stages were more productive than the upper stages during the daytime because of the internal delays. The highest CBA of 10.35 produced the most distillate per day in the winter season, such that for stages 1 to 4, it was 10.49, 6.81, 5.80, and 4.73 kg/m^2, respectively. The enhanced productivity for the highest CBA was due to an increased thermal energy input rate. However, in the summer season, the CBA of 3.45 supplied sufficient heat to start and sustain the desalination process. Increasing CBA from 3.45 to 6.90 and 6.90 to 10.35 enhanced the distillate production by 48% and 23%, respectively.

Moreover, the larger CBA caused the HTF to boil, increasing the heat losses. The augmentation of three FPSCs caused the SW temperature in all the stages to be almost equal, which ceased the desalination process. Lastly, increasing the number of stages inversely affected the daily cumulative distillate yield. There are other studies on the annual performances of solar stills [17, 18].

Various studies found in the literature reported annual productivities of different solar stills, which correlated with prevailing meteorological conditions. The current work aims to inform on the year-round productivity correlation of the standalone vapour-based MSS-SS with new configurations under given meteorological conditions [19]. The experimental analysis focuses on the MSS-SS seasonal cumulative productivity, rate and mode of thermal energy, stages distillate yield trends, the effects of the low thermal inertia of water mass, the trends and effects of heat recovery, and SW preheating in the condensing tower. The attention is given to the five stacked stages to the exclusion of the BSS except to refer to its effects.

2. Description of the Vapour-Based MSS-SS

A schematic diagram of the test rig illustrating the external SW tank, stages 1 and 2, basin-passive solar still, evaporator, secondary SW tank, and the solar panel is shown in Figure 1. The condensing tower covers and the stage trays were made from 0.9 mm thick aluminium sheets. The stage trays were inclined at 8° from the horizontal to allow for the distillate collection [16]. The trays were also bent into V-shape longitudinally at the centre for efficient distillate collection. Various holes of 15 mm diameter were drilled through the trays near one end to allow vertically mounted vapour make-up tubes to pass through stages. The evaporator made from food-grade stainless steel supplied the vapour to the stacked stages through the vapour make-up tubes. The SW at room temperature was supplied from the external tank through a thin-walled transparent tube to the BSS.

The BSS was the first SW receiver where it was initially preheated directly by the sun rays. It was then supplied to the rest of the stages via the zig-zagged SW tube made from copper material with an external diameter of 15 mm. The systems' layout was aimed at maximising heat exchange interactions between the vapour and the SW. This interaction is depicted by the red and blue arrows shown in stage 1, where the vapour eventually condensed due to a larger temperature difference. The preheated SW was stored in the secondary SW tank before transferring it into the evaporator for further heating and evaporation. Two float valves, one installed in the BSS and the other, in the secondary SW tank, controlled the SW flow throughout the system. The hot and cold tubes transported SW between the evacuated tube solar collectors (ETSCs) and the evaporator, where the SW-vapour separation occurred. This layout was to enhance the vapour production in the evaporator. The vapour from the evaporator was distributed amongst the five parallel vapour make-up tubes delivering the vapour into the stages [20]. The SW in the zig-zagged SW tube was used to absorb the latent heat of condensation given away by the condensing vapour in the stages. The distillate was collected from the distillate collecting points and direct it to the storage containers.

Furthermore, Figure 2 shows the view of the condensing tower with the five stacked stages. The zig-zagged tube travelled through each of the five stages. It made several passes in each stage for heat recovery and SW preheating. The quantities of SW in the evaporator and the secondary SW tank at any time were 1.7 kg and 2.8 kg, respectively. In addition, to preheating the SW, the BSS also produced its distillate. The condensing tower and the ETSCs were positioned northwards for maximum solar radiation collection. The vapour-based MSS-SS stages had no SW in contact with the stage trays; it relied on the SW in the zig-zagged SW tube to condense the vapour. Moreover, the system had relatively minimal SW in the condensing tower compared to the existing MSS-SS found in the literature.

3. Operating Principle of the System

Before starting the first operation after commissioning, the system was primed with SW to ensure that all tanks, tubing lines, and the evaporator were filled. Furthermore, the SW was directly heated by the ETSCs manifolds, as no HFT was used. A view illustrating the condensing tower and the ETSCs connected in series is shown in Figure 3. The operation of a fully primed system started in the ETSCs and the BSS simultaneously at the start of the day as the solar incidence increased.

Solar radiation striking the surfaces of the ETSCs increased both the temperature and the pressure of SW in the ETSCs manifolds, which caused it to escape the manifolds to equalise. Since the nonreturn valve (swing type) allowed only one-directional flow, the SW was forced to the escape path leading it to the evaporator through the hot SW tube (Figure 1). Upon entering the evaporator, the separation of the denser SW and the lightweight vapour occurred owing to the orientation of the hot SW tube's outlet. The denser SW sank to the bottom of the evaporator while the light vapour ascended toward the vapour make-up tubes. Meanwhile, the SW that escaped the manifolds left a vacuum, which then sucked the next batch of SW for heating in the manifolds. The cold SW tube, slightly tilted at an angle from the horizontal surface (Figure 3), supplied additional SW from the evaporator. When the second batch escaped the manifolds due to increasing temperature and pressure, the next batch was sucked in, and the process repeated throughout the day. Therefore, the SW was circulated consistently between the evaporator and the ETSCs throughout the day. The SW circulation depended on the solar intensity; at the low solar intensities, SW circulated impulsively (start and stop). However, the impulsive action ceased at the high solar intensities, and the flow assumed a continuous mode translating to enhanced vapour production.

Moreover, the lightweight vapour distributed amongst the five parallel vapour make-up tubes condensed upon entering the stages due to a significant temperature difference between itself and the condensing surfaces. Simultaneously, the condensing vapour preheated the SW flowing in the zig-zagged tube by releasing the latent heat of condensation. The preheated SW flowing in the zig-zagged SW tube was then stored in the secondary SW tank. Given the stacked stages' layout and, in theory, the SW in the zig-zagged tube was preheated each time it passed a stage. The preheated SW in the secondary tank replenished diminishing SW in the evaporator through the SW transfer tube (Figure 1) due to evaporation.

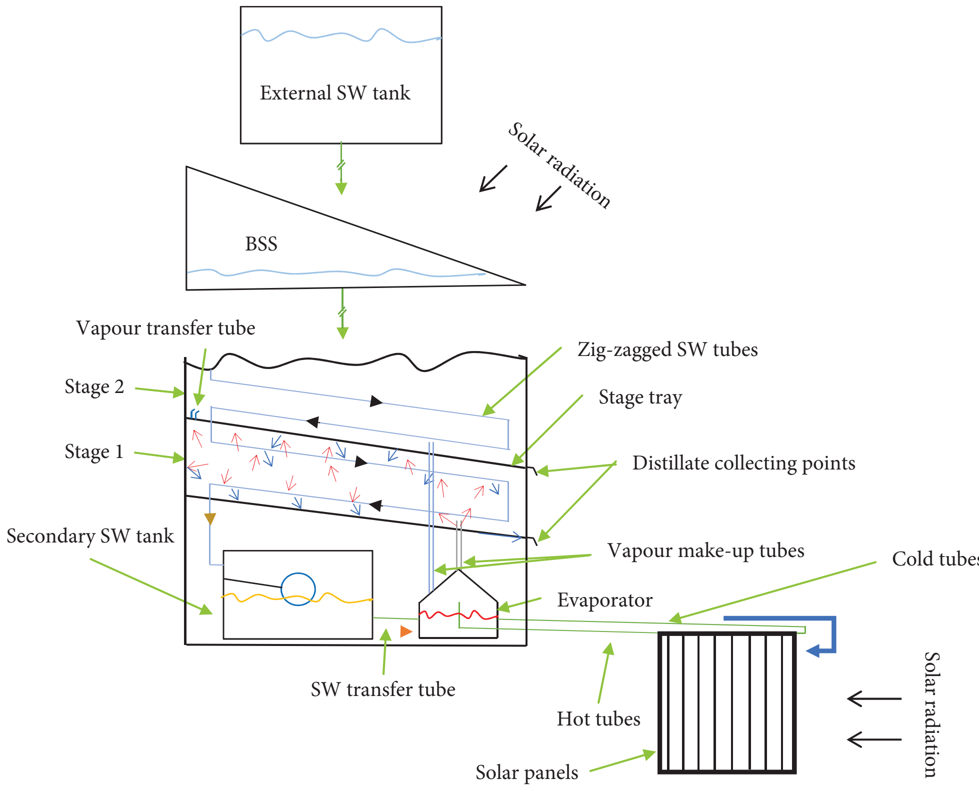

Figure 1: MSS-SS schematic diagram.

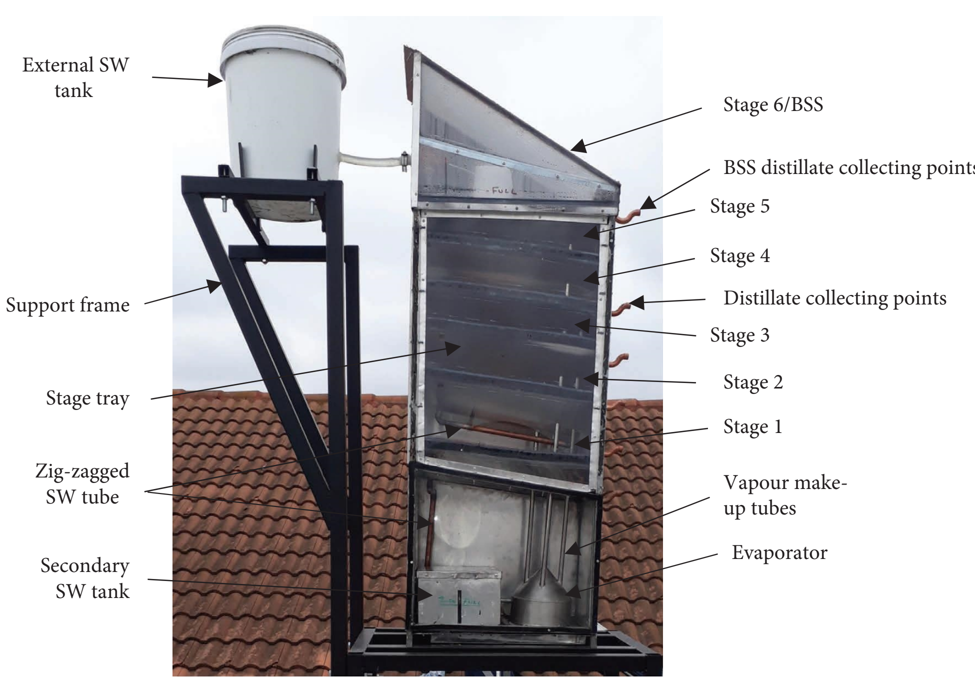

Figure 2: Vapour-based MSS-SS.

Furthermore, the vapour transfer tubes (Figure 1) safeguarded against pressure build-up in the stages by transferring the excessive vapour sequentially to the stage directly above. The distillate trickled down the tilted trays upon condensing and was collected at the distillate collection points. The BSS produced its distillate through direct and indirect heating by sunrays and vapour in stage 5 and the distillate was collected from the distillate collecting point

Figure 3: ETSCs and condensing tower view of the vapour-based MSS-SS.

(Figure 2). There are several factors affecting and influencing MSS-SS that can be quantified comparatively between the vapour-based MSS-SS and other existing MSS-SS systems [19].

4. Experimental Procedure

The vapour-based MSS-SS was tested at Cape Peninsula University of Technology (CPUT) in Cape Town, South Africa. The experimental tests started in September 2020 through June 2021, covering all four-year seasons. The test rig and the ETSCs were positioned northwards for a maximum solar incidence exposure. Data logging of the temperature was performed 24 hours a day using a BTM-4208SD, 12-channel data logger. K-type thermocouple probes were used, and those probing SW in the stages were attached to the outer surface of the thin-wall zig-zagged tube. There were 12 probes, nine surface-type probes, and three immersion-type probes.

The solar radiation, wind velocity, and ambient air temperature were logged using the HP2000 wireless weather station model for 24 hours daily. The distillate was collected using a graduated cylinder with a maximum capacity of 1000 ml (1 litre). The distillate collection was done each morning before the start of the operation to avoid any disruptions. Furthermore, the SW was recirculated in the evaporator and ETSCs for up to 14 days without disposing of the brine solution. However, the collection period was reduced during seasons with the high solar intensities, which caused high evaporation rates in the evaporator.

Moreover, brine collection was also done in the morning to avoid losing heat through hot brine. The instruments used are shown in Table 1 with their names, make/model, range, accuracy, and error data. The minimum error occurring in any device is the ratio of its least count to the minimum measured output value [16].

5. Results and Discussion

The latitude and longitude of Cape Town are 33.9249°S and 18.4241°E, respectively. The series connected ETSCs were tilted at approximately 56° from the horizontal and facing northwards. Moreover, due to the large data sets on measured parameters (solar radiation, wind velocity, and ambient air temperature) over the duration of the experimental study, daily global solar radiation on a horizontal surface was averaged and categorised into three groups. The average ranges were from 0 to 199 W/m^2, 200 to 399 W/m^2, and 400 to 600 W/m^2 for low, moderate, and high ranges, respectively. Furthermore, daily global solar radiation on a horizontal surface was used to numerically estimate the total solar radiation on the tilted ETSCs with a total aperture area of 1.8 m^2. Figure 4 shows the daily average solar radiation variations throughout the study (10 months).

The vapour-based MSS-SS was productive on consecutive days for most of the period under discussion. However, the rainy season, prevalent in June, reduced and sometimes halted the desalination process altogether due to low solar intensities. Furthermore, days with little to no operational disruptions were selected for discussion.

5.1. Low Daily Average Solar Radiation. Results from typical days of this range of 0 W/m^2 to 199 W/m^2 are shown in Table 2, with nonmeasurable (NM) denoting the insignificant distillate production. Days in this category were predominantly in early spring, late autumn, and winter seasons. These days were characterised by cooler surrounding temperatures (column 9) with partial or complete cloud cover. It was observed that the system's productivity increased gradually with an increase in the average solar radiation, as shown in Table 2. The condensing tower was thermally insulated with a 20 mm thick polystyrene insulation material, except on the 6th of November 2020.

Table 1: Error data for instruments used.

Instrument name	Make/model	Range	Accuracy	Error (%)
(1) 12 channels temp, data logger	BTM-4208SD	−50 to 999.9°C	± (0.4% + 0.5°C)	1.5
(2) Thermocouples				
(2.1) Surface probes	Type K	−100 to 250°C	± 0.1°C	0.5
(2.2) Immersion probes	SJ-100/K505B3	−190°C to 260°C	± 0.1°C	0.5
(3) Wireless weather station				
(3.1) Wind speed	HP2000	0 to 50 m/s	± 1 m/s (speeds <5 m/s) ± 10% (speeds >5 m/s)	4.3
(3.2) Ambient air temperature sensor		−30 to 65°C	± 1°C	2.1
(3.3) Solar radiation		0 to 3157 W/m^2	± 15%	3
(4) Graduated cylinder	Simax	0 to 1000 ml	± 10 ml	10

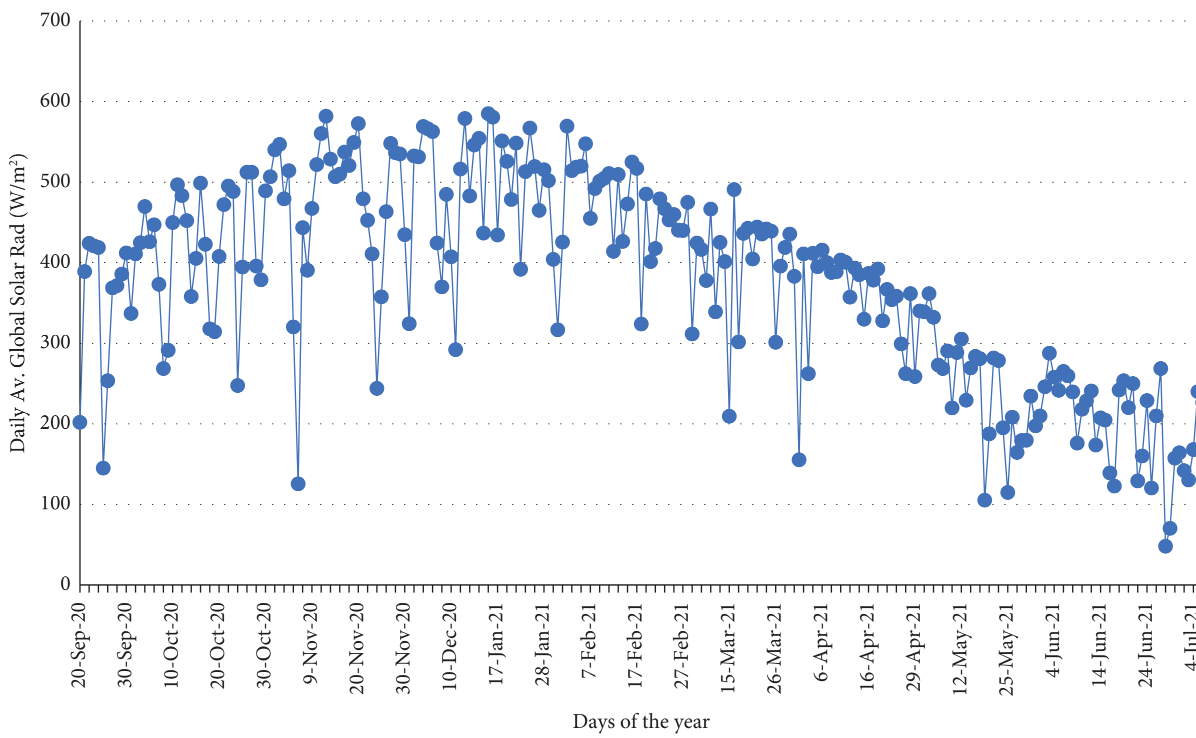

Figure 4: Daily average global solar radiation on a horizontal surface.

Table 2: Various parameters of the vapour-based MSS-SS under low average conditions.

0	1	2	3	4	5	6	7	8	9	10
Date	St 1	St 2	St 3	St 4	St 5	BSS	Av. daily sol. rad.	Max. daily sol. rad.	Av. daily ambient temp.	Av. daily wind velocity
	Distillate yield (ml)						(W/m^2)		(°C)	(m/s)
06-Nov-20	NM	NM	NM	NM	NM	NM	125.6	260.5	15.3	3.3
23-Jun-21	NM	NM	NM	NM	NM	NM	160.2	504.9	16.7	0.9
29 May-21	560	100	170	30	250	80	179.5	586.9	16.9	2.1
31 May-21	250	30	120	20	30	130	197.6	566.1	14.7	1.6

The solar radiation curve patterns demonstrated similar trends as reported in the literature on a daily, monthly, and seasonal basis, as shown in Figure 4. The evaporator SW temperature curves are shown in Figure 5 for the days tabulated in Table 2. These curves were closely correlated with the prevailing daily solar radiation curves and demonstrated an impulsive mode of the thermal energy input [21]. The figure shows that the insufficient heat was collected for lower daily average solar radiation to cause the evaporator SW temperature curve to react, such as on the 6th of November 2020, despite the condensing tower being insulated. However, with a gradual increase in the daily

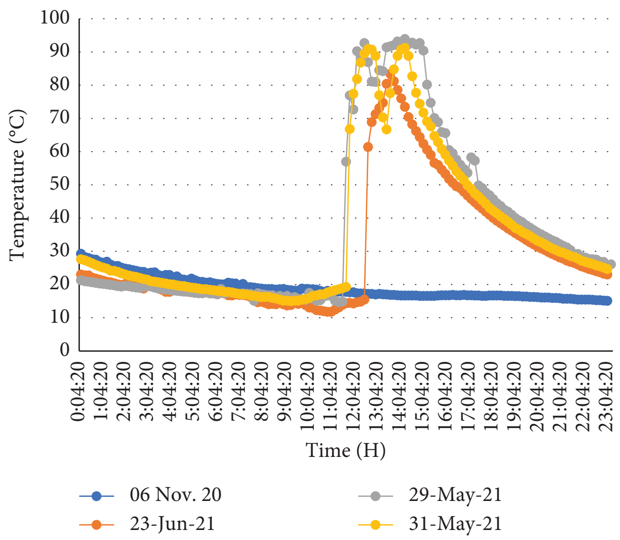

Figure 5: Evaporator SW temperature on various days under low average solar radiation.

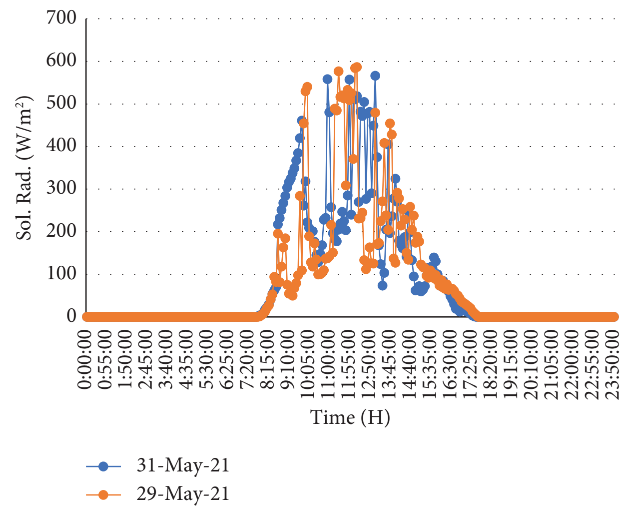

Figure 6: Solar radiation curves under low average daily solar radiation.

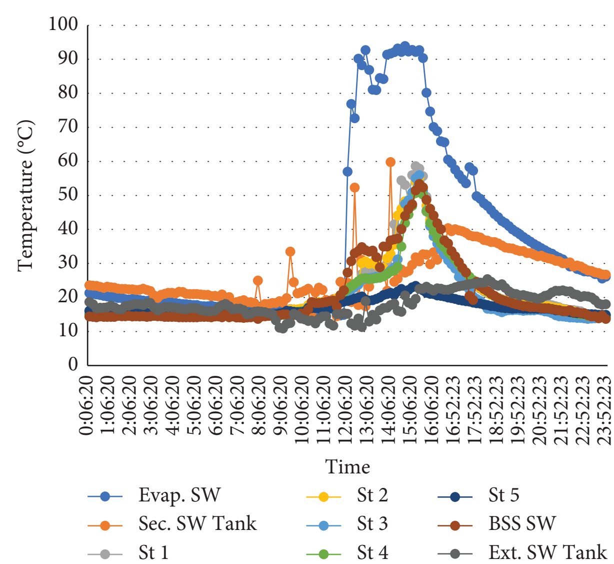

Figure 7: SW temperature curves for the 29th of May 2021.

average solar radiation, momentary reactions indicated increased heat collection by the ETSCs. The days in this range signified the minimum operating conditions for the vapour-based MSS-SS.

Despite the minimum operating conditions, the following aspects were observed based on Figures 5 and 6. (1) Due to the low thermal inertia of water mass in the ETSCs manifolds, the SW temperature curves increased sharply almost vertically to approximately 90°C; this was proportional to the rate of heat supply. (2) Such SW temperature patterns were consistent with maximum vapour production in the evaporator. (3) The low thermal inertia of water mass adversely affected its thermal energy storage capacity, thus, becoming sensitive to the varying solar radiation intensities. The correlation can be made between the thermal energy input in Figure 7 with the evaporator SW temperature behaviours in Figure 6. It can be observed that the evaporator SW temperature curves declined almost simultaneously with the solar radiation later in the day, and its temperature dropped to below 30°C by midnight. Lastly, as displayed in Table 2, ambient conditions directly influenced the low thermal inertia of water mass as the condensing tower was uninsulated. (4) Vapour supply to the stages through the parallel vapour make-up tubes was grossly uneven, as shown by the stage's distillate yields in Table 2. The pressure build-up may have influenced this in some stages due to excess vapour and insufficient cooling and condensation of the vapour by the SW in the stages. It may also be the position of the vapour make-up tubes mounted on the evaporator. (5) The mode of the thermal energy supply was predominantly impulsive than continuous, suggesting insufficient energy to sustain the desalination process characterised by low productivity. (6) At this range of average solar radiation, there was an apparent delay in the vapour delivery to the stages through the vapour make-up tubes from the evaporator. This mainly resulted from the cold system's components, which caused the temperature gradient between the vapour and the tube's inner wall to be greater. This caused the vapour to condense prematurely in the tubes before reaching the stages. The cold tube walls created a thermal boundary layer which prevented the vapour in bulk motion from reaching the stages. Thermal equilibrium in the tubes was a prerequisite and must be maintained for the vapour to flow past without condensing. A larger temperature difference or gradient caused higher convective heat transfer between the vapour and the tubes' walls, reducing the vapour temperature and thus causing it to condense [22].

For example, the 29th of May 2021 is discussed in Figure 7, which shows the SW temperature curves in all the compartments of the condensing tower. It can be observed that the vapour supply pattern reflected by the distillate yields in Table 2 was predominant such that stage $1 > 5 > 3 > 2 > 4$. However, the SW temperature curve pattern was such that stage 1 > 3 > 2 > 4 > 5, showing some degree of correlation between the SW temperature in the stages to the vapour supply patterns. This behaviour corresponds with the BSS's sequential SW preheating and heat recovery. At this average solar radiation range, stages productivity and temperature profiles followed the above trends; but at times, stage 2 or 3 was the most productive. In contrast, stage 4 remained the least productive, no matter the change in pattern. The rationale for stage 5 temperature curve behaviour was that it was located adjacent to the BSS, which contained a pool of SW. Therefore, the bulk of the vapour condensation was aided by the BSS SW and the SW in the zig-zagged tube in stage 5. Thus, in addition to direct heating in the BSS, the SW was also heated by the vapour condensing on the underside of the BSS. Figure 7 shows that the BSS SW temperature curve was similar to stage 4.

The total cumulative SW preheating and heat recovery was reflected by the SW temperature variation in the secondary tank, as shown in Figure 7 by the (Sec. SW tank) curve. Furthermore, the SW temperature difference between the external and secondary tank indicated the extent to which the SW was preheated as it flowed through the system. On average, this temperature difference was 4.5°C, 8.4°C, 9°C, and 9.8°C for the 6th of November 2020, 23rd of June 2021, 29th of May 2021, and 31st of May 2021, respectively. Moreover, the cumulative distillate yields for the condensing tower were NM, NM, 1190 ml, and 580 ml on the 6th of November 2020, 23rd of June 2021, 29th of May 2021, and 31st of May 2021, respectively.

5.2. Moderate Daily Average Solar Radiation. The days in this range of 200 W/m^2 to 399 W/m^2 displayed the productivity patterns in Table 2, where no NMs were recorded. These days were mainly found in all the seasons except for the summer season. These days were characterised by occasional cloud cover and clear skies. Furthermore, the autumn season coincided with the calibration of the temperature data logger instrument. Hence, days in this season are not included in the discussion. The 20 mm thick thermal insulation material was used only on the 29th of September 2020.

Figure 8 shows distinct curves from Figure 5, indicating an increased thermal energy collection by the ETSCs, thus, increasing thermal energy input. It can be noted from Figure 8 in relation to Figure 5 that the sharp increase of the evaporator SW temperature curves to approximately 90°C occurred 2 hours earlier in the morning. The low thermal inertia of water mass and increased solar intensities resulted in the patterns in Figure 8. The SW temperature curves were maintained at approximately 90°C for extended periods, translating to increased vapour production.

Furthermore, despite thermal insulation on the body of the condensing tower on one of the days, Figure 8 shows that the SW temperature curves dropped rapidly later in the afternoon to below 30°C by midnight. This behaviour was linked to the low thermal inertia of water mass, which indicated that the desalination process was not prolonged during off-sunshine hours. The six (6) aspects observed in subsection 5.1 are consistent and can be further observed under this average daily solar radiation range.

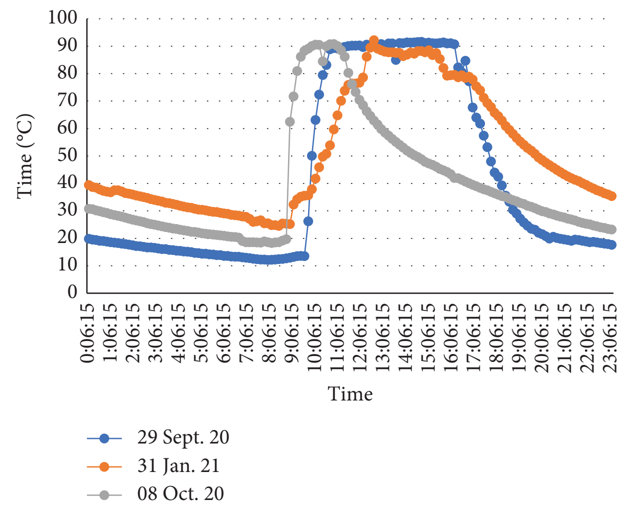

Figure 8: Evaporator SW temperature on various days under moderate average solar radiation.

However, there were notable changes in these aspects relating to the SW temperature behaviours with increasing solar intensities, while some remain the same. The three changed aspects under this range can be described as follows: (1) The system's sensitivity due to the low thermal inertia of water mass diminished, as shown in Figure 9 in relation to Figure 8. It can be observed that despite the rapid fluctuations in Figure 9, no similar fluctuations were observed for the evaporator SW temperature curves. This was attributed to an increased rate of thermal energy input, given the area under the curves compared to Figure 5. Therefore, the mode of thermal energy input was continuous, suggesting sufficient heat to sustain the desalination process. (2) It is plausible to conclude that the delay in the vapour make-up tubes was reduced, given the heat intensity in the evaporator and the tubes. However, the rapid decline in the SW temperature with diminishing solar intensities remained consistent with those reported in subsection 5.1. (3) The SW temperature patterns were such that stage 2 > 3 > 4 > 1 > 5, as shown in Figure 10 as an example. This pattern had changed entirely from the original one reported in subsection 5.1. Unlike the previous pattern in subsection 5.1, the SW preheating and heat recovery were random and according to the vapour supply from the evaporator. This suggested that the increased heat input was sufficient to diminish the BSS SW preheating effects regardless of the BSS preheating contributions. Furthermore, the experimental observations showed a decreased temperature difference between the evaporative and condensing surfaces [9]. This critically reduced temperature difference and threatened thermal damage conditions [23].

The vapour supplied pattern from the evaporator reflected by the distillate yields in Table 3 was such that stage 5 > 3 > 2 > 1 > 4. Despite the random nature reflected by the above trends, the following can be noted: the stage productivity was inversely proportional to its SW temperature; hence, stage 5 was the most productive, stages distillate yields and SW temperature trends varied with the rate of

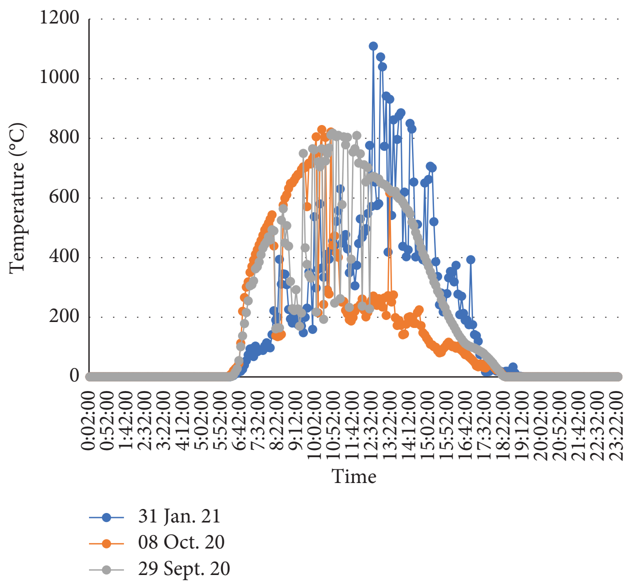

FIGURE 9: Solar radiation curves under moderate average daily solar radiation.

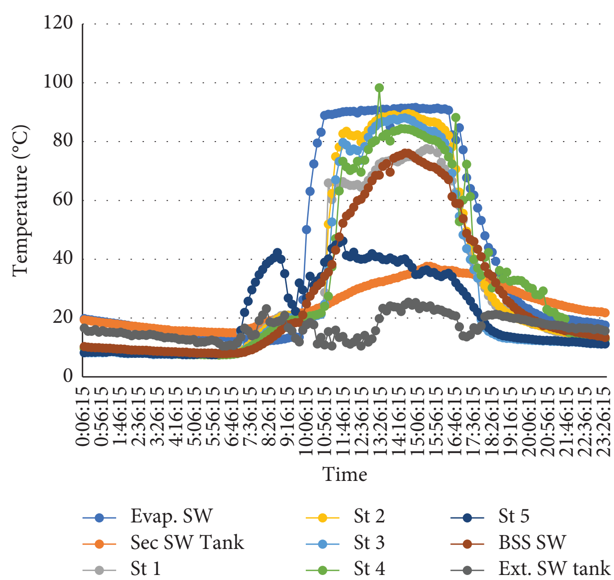

FIGURE 10: SW temperature curves for the 29th of September 2020.

thermal energy input, stage 4 remained the least productive stage regardless of the rate of heat input, and stages 1 to 4 had insufficient feedwater to cool down and maintain moderate temperatures suitable for the continued desalination process; hence, thermal damage was imminent.

The secondary tank curve reflected the cumulative SW preheating and heat recovery in the secondary tank in Figure 10. The SW temperature difference between the secondary and external tank was 7.7°C, 11°C, and 11.2°C on the 29th of September 2020, the 8th of October 2020, and the 31st of January 2021, respectively. There was a slight increase in the cumulative SW preheating and heat recovery compared to the low range of daily average solar radiation. The cumulative daily distillate yields for the condensing tower were 5460 ml, 5330 ml, and 6090 ml, respectively, for the corresponding dates above.

5.3. High Daily Average Solar Radiation. This range was the highest, with the lower and upper limits of 400 W/m^2 to 600 W/m^2, respectively. As the solar intensities increased further away from zero, the NM quantities disappeared, since the system was consistently productive. These days were mainly found in the late spring and summer seasons. They were characterised by clear skies, higher ambient temperatures, and wind velocity, as shown in Table 4. In this range, the continuous mode of thermal input, critical temperature difference reduction between the evaporative and condensing surfaces, and the absence of the insulation material were normal.

Figure 11 shows a maximum vapour production curves for up to 8 hours daily. The SW temperatures of approximately 90°C were maintained, suggesting continuous flow in the evaporator and the ETSCs. It can further be noted that the sharp curve increase occurred about 2 hours earlier than those in subsection 5.2 and 4 hours earlier than those in subsection 5.1. The full advantage of low thermal inertia mass of water was demonstrated. Furthermore, the favourable ambient conditions caused the SW temperatures to be at 30°C in the morning before the sharp curve increased and above 44°C by midnight at the end of the day. This meant that the desalination process continued long after sunset, aiding in vapour production.

The evaporator SW temperature could be as high as 58°C around 8 PM as the solar radiation ceased, as shown in Figures 11 and 12. Furthermore, the system's sensitivity diminished with increasing solar intensities, thus, ensuring the continuous mode of thermal energy supply. The area under the curve had further increased, as demonstrated in Figure 12, translating to a further increase in heat supply to the condensing tower.

Figure 13 shows the SW temperature for the 23rd of November 2020. It is observable from Figures 12 and 13 and Table 4, showing the average ambient temperature and wind velocity, that there was a pronounced drop in the solar radiation curve. This drop was translated to Figure 13 as the SW temperatures dropped around noon. This reflected a decrease in vapour production in the evaporator. Therefore, it can be concluded that the system's sensitivity only diminished for the solar radiation fluctuations occurring for short periods, but it was visible for the pronounced and prolonged fluctuations. Furthermore, these fluctuations and drops prevented thermal damage conditions and thus, did not affect the desalination process. The SW temperature trends were such that stage $1 > 2 > 3 > 4 > 5$, indicating a similar pattern to those reported under subsection 5.1. Moreover, the vapour supply trend was such that stage $5 > 3 > 2 > 1 > 4$, precisely like those reported in subsection 5.2. The vapour supply trend suggested that despite this day falling under high daily average solar radiation, the solar radiation behaviour was equivalent to the moderate range of average daily solar radiation.

Furthermore, Figure 13 shows that the secondary SW tank reached temperatures of 55°C, much higher than those reported in the previous subsection. This cumulative SW

Table 3: Various parameters of the vapour-based MSS-SS under moderate conditions.

0	1	2	3	4	5	6	7	8	9	10
Date	St 1	St 2	St 3	St 4	St 5	BSS	Av. daily sol. rad.	Max. daily sol. rad.	Av. ambient temp.	Av. wind velocity
	Distillate yield (ml)						(W/m^2)		(°C)	(m/s)
08-Oct-20	990	1190	1100	650	940	460	268.8	829.3	18.6	1.2
31-Jan-21	980	1320	1200	580	1440	570	316.9	1109	21.8	3.8
29-Sept-20	1020	1040	1050	590	1280	480	385.7	817.7	15.5	3.2

Table 4: Various parameters of the vapour-based MSS-SS under high conditions.

0	1	2	3	4	5	6	7	8	9	10
Date	St 1	St 2	St 3	St 4	St 5	BSS	Av. daily sol. rad.	Max. daily sol. rad.	Av. ambient temp.	Av. wind velocity
	Distillate yield (ml)						(W/m^2)		(°C)	(m/s)
23-Nov-20	1020	1050	1130	690	1220	630	411	1165	18.5	2.9
08-Feb-21	1120	1370	1440	740	1350	560	492.2	1031	23.5	6
12-Dec-20	1040	1210	1280	870	1340	730	516.4	986.9	20	4.2
13-Jan-21	760	1550	1630	910	1880	1060	585	892	29.3	3.1

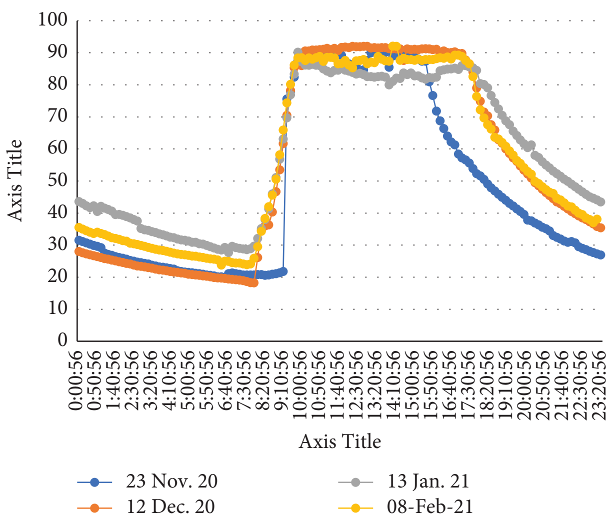

Figure 11: Evaporator SW temperature on various days under high average solar radiation.

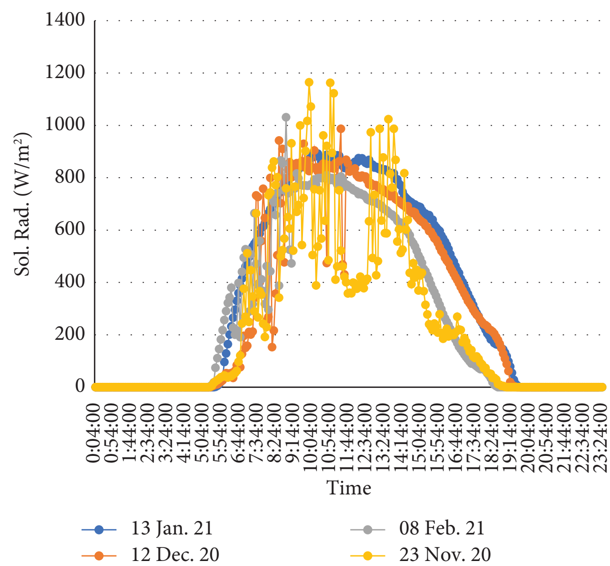

Figure 12: Solar radiation curves under high average daily solar radiation.

preheating indicated a noninterrupted vapour production in the evaporator as the SW in the secondary tank was heated to elevated temperatures. Furthermore, it suggested that the energy required to heat and vaporise SW in the evaporator was lessened. However, on average, the SW temperature difference between the secondary SW tank and the external tank was 10.2°C, indicating that the extent of preheating was virtually like those in subsection 5.2. It is observable from Figure 13 compared to Figure 10 that the external SW temperature curve was higher, influenced by the prevailing ambient conditions in the summer season.

A further increase in the rate of thermal energy input under the continuous mode of thermal energy resulted in the SW temperature behaviours in Figure 14. The least productive stage (stage 1) exceeded that of the evaporator SW. It

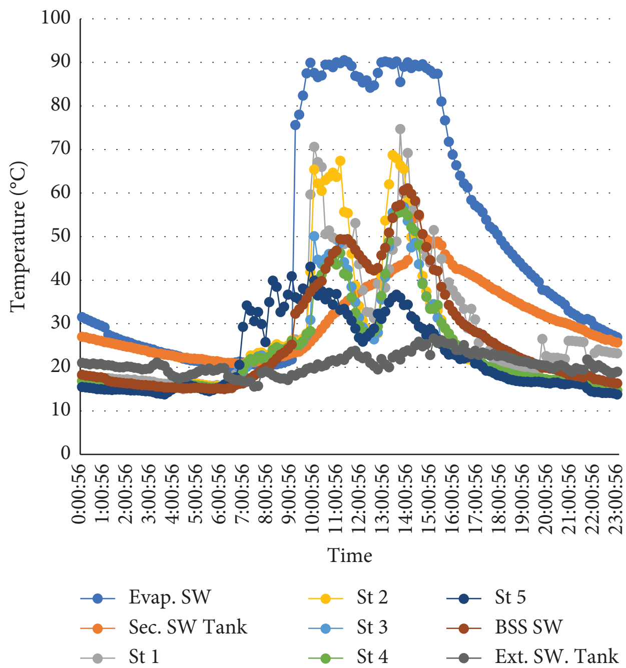

Figure 13: SW temperature in the condensing tower under high average conditions (23-Nov-2020).

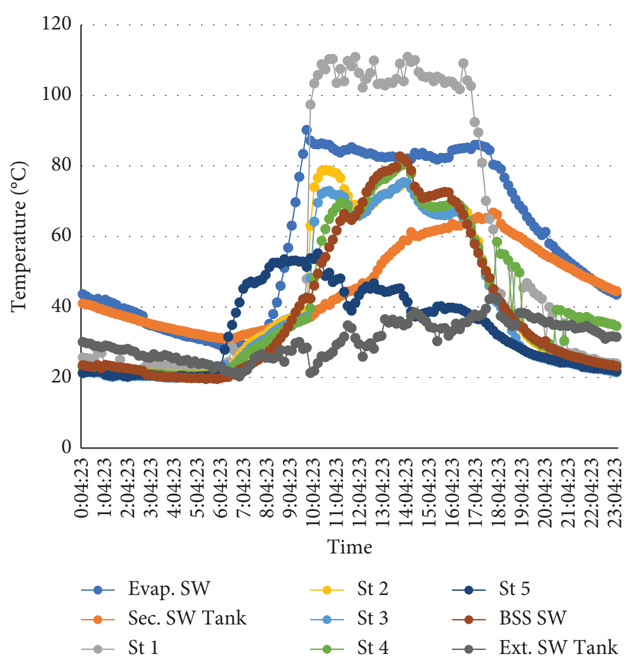

Figure 14: SW temperature in the condensing tower under high average conditions (13 Jan 2021).

is worth noting that the temperature probe in this stage may have also been reading the zig-zagged SW tube surface temperature. It is agreeable that this stage operated at the thermal damage conditions, and its temperature was inconsistent with other stages. Moreover, the vapour may have been leaking from stage 1 to the surroundings in addition to transferring it to stage 2 via the vapour transfer tube (Figure 1). The SW temperature trends were such that stage $1 > 4 > 3 \approx > 2 > 5$ were slightly similar to those in subsection 5.1. However, unlike those in subsection 5.1, this trend demonstrated a lack of productivity for those stages operating close to or at thermal damage conditions. This demonstrated that the stage productivity was inversely proportional to its SW temperatures. Moreover, the productivity trend was such that stage $5 > 3 > 2 > 4 > 1$, substantiating the finding of insufficient vapour condensation for stages maintaining elevated temperatures. Moreover, due to favourable ambient conditions, the SW in the stages and the evaporator were above 20°C at midnight at the end of the day.

The heat recovery and SW preheating effects were driven by the vapour delivered from the evaporator, as demonstrated by Figure 14. The figure also shows that the direct heating in the BSS had increased to a maximum of 83°C, signalling an increased heat input rate which translated to increased vapour production. Furthermore, the cumulative SW preheating and heat recovery resulted in the secondary SW temperature reaching at 66.8°C, as shown in Figure 14. The absence of insulation material and wind velocities in Table 4 contributed to the cooling down of the condensing tower, thus, increasing the condensation process.

On average, the temperature difference between the secondary tank and the external tank was 15.5°C, 12.4°C, and 14.1°C on the 13th of Jan. 2021, 8th of Feb. 2021, and 12th Dec. 2020, respectively. The daily cumulative distillate yields were 5740 ml, 6580 ml, 6470 ml, and 7790 ml, respectively. The vapour-based MSS-SS seasonal productivity was linked to the rate and mode of thermal energy input. The daily solar radiation curve progression dictated the mode of the thermal energy input, which drove the ability of SW cooling effects in the condensing tower. Therefore, under the high daily average solar radiation range where continuous modes were assumed, the low thermal inertia of water mass was unable to cool down and condense the vapour in the condensing tower without causing thermal damage conditions.

5.4. Seasonal Productivity. Figure 15 shows the stages' distillate yield trends for a year-round experimental study. There was a significant increase from the low average range of the solar radiation to the moderate range by 348% between 1190 ml and 5330 ml. These values corresponded with a 36% increase in the average solar radiation from 197.6 W/m^2 to 268.8 W/m^2. It suggested that the MSS-SS was most suitable to operate at the lower values of the moderate daily average solar radiation range with the insulation material. However, in the upper values of this range, as demonstrated by Figure 10, the condensing tower approached thermal damage conditions when insulated. Therefore, the insulation material was unsuitable for the late spring, summer, and early autumn seasons, where moderate and higher daily average solar radiation was prevalent. It implied that the optimum rate of thermal energy when the condensing tower was insulated was the lower values of the moderate range. A further increase to the high range necessitated the augmentation of the TES to minimise heat losses.

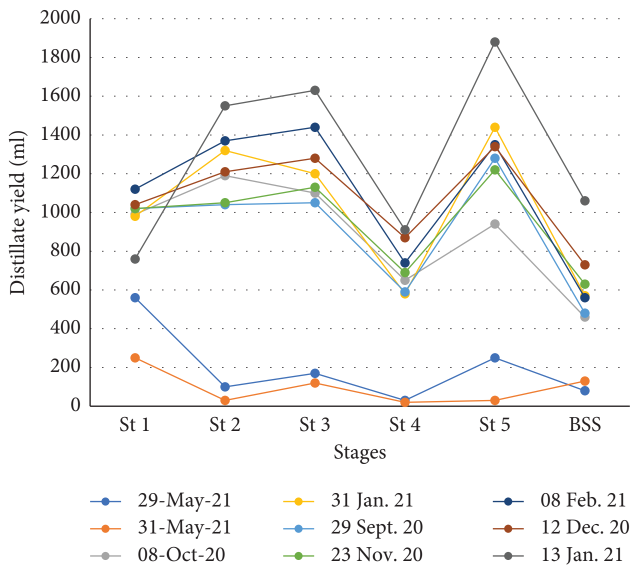

Figure 15: Year-round distillate yield trends.

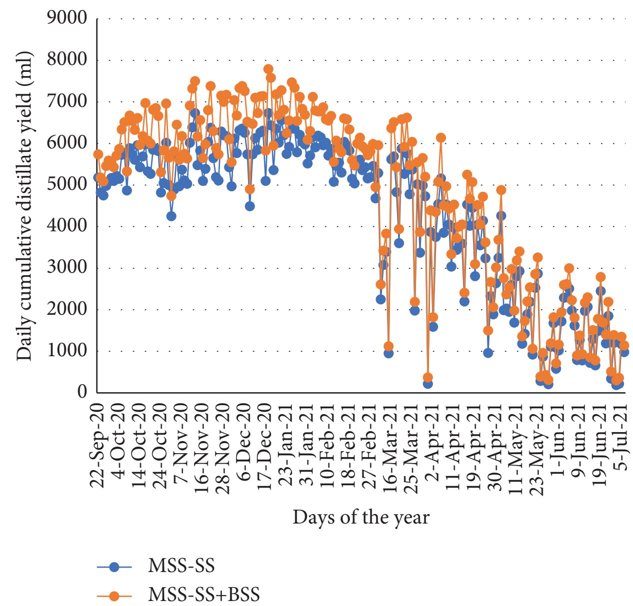

Figure 16: Year-round daily cumulative distillate yield trends.

Moreover, Figure 15 shows that the further increase in the thermal energy input rate did not significantly impact the distillate yield. For instance, increasing the average daily solar radiation by 152% enhanced the daily cumulative distillate yield by only 43%, from 5460 ml to 7790 ml on the 29th of September 2020 and the 13th of January 2021, respectively. This may be associated with increased heat losses through the walls and undetected vapour leaks to the surroundings caused by thermal damage. However, there was an observable pattern in the stages of distillate yields. That is, the bottom stages experienced enhanced productivity at a low daily average range of solar radiation. The pattern was random at moderate to the high average daily solar radiation, but stages $5 > 3 > 2$ were the most productive, respectively. The study's main findings were as follows: (1) The thermal boundary layer was not easily overcome for the MSS-SS at a low daily average range of the solar radiation. (2) Thermal energy requirements were low due to the low thermal inertia of water mass. Still, it was susceptible to thermal damage conditions. (3) The system had a larger CBA ratio as it experienced thermal damage at the upper values of the moderate daily average solar radiation. (4) The stages' distillate yield trends changed with changing modes and increasing rates of thermal energy input. The significant cumulative distillate yield decline of 80.5% from 6090 ml to 1190 ml occurred on the transition between the moderate range to the low range of daily average solar radiation. Only a 21.8% decline occurred between the high and moderate ranges of daily average solar radiation from 7790 ml and 6090 ml.

Figure 16 shows the daily cumulative distillate yield patterns throughout the experimental tests period, excluding unproductive days denoted by NM in Table 2. Daily cumulative distillate yield trends from the vapour-based MSS-SS over the year's four seasons were consistent with those discovered in the literature. Low daily cumulative distillate yields coincided with low rates of thermal energy inputs, which were affected by prevalent cloud cover and low peak values, amongst other factors (Figure 4). Even though the BSS was not the focus of the study, Figure 16 shows that its contribution in the spring and summer seasons was most considerable. The autumn season's beginning shows a sharp decline in daily cumulative distillate yield. This behaviour was associated with the accumulation of cloud cover, which reduced direct solar radiation reaching the ground.

6. Economic Analysis

Economic analysis was based on the correlation reported in the studies of El-Bialy et al. [24], Fath et al. [25], and Adhikari et al. [26]. These analyses are considered for each day discussed in Section 5. Equations (1-8) were used to determine the cost implications for using the vapour-based MSS-SS to produce freshwater and are defined as follows. When equipment depreciates, some value is left; therefore, a salvage value (S) is one parameter. The design and overall construction of a solar still involve costs, which are the present capital cost (P).

Furthermore, annual costs (ACs) include the cost of ownership, operation, and land rental. The cost of producing freshwater per litre (CPL) is estimated by considering all operational costs. A sinking fund factor (SFF) accounts for the system's depreciation over time and calculates the equipment's future value.

The fixed annual cost (FAC) is the fixed cost of the equipment operation. The FAC does not change with the CPL. The capital recovery factor (CRF) is the ratio of constant return on the value of the equipment over the equipment's lifetime. Annual maintenance costs (AMCs) are equipment upkeep costs and are generally estimated to be a fraction of the FAC. The yearly interest and number of

Table 5: CPL based on the daily distillate yield of the vapour-based MSS-SS.

0	1		2		3	
Date	Daily cumulative dist. yield		Annual dist. yield (M)		Cost per litre (CPL)	
	MSS-SS	MSS-SS + BSS	MSS-SS	MSS-SS + BSS	MSS-SS	MSS-SS + BSS
	(Litres)				South African rands (R)	
06-Nov-20	—	—	—	—	—	—
23-Jun-21	—	—	—	—	—	—
29 May-21	1.11	1.19	288.6	309.4	28.45	26.54
31 May-21	0.45	0.58	117	150.8	70.17	54.44
11 June-21	1.97	2.17	512.2	564.2	16.03	14.55
08-Oct-20	4.87	5.33	1266.2	1385.8	6.48	5.92
31-Jan-21	5.52	6.09	1435.2	1583.4	5.72	5.19
29-Sept-20	4.98	5.46	1294.8	1419.6	6.34	5.78
23-Nov-20	5.11	5.74	1328.6	1492.4	6.18	5.50
08-Feb-21	6.02	6.58	1565.2	1710.8	5.25	4.80
12-Dec-20	5.74	6.47	1492.4	1682.2	5.50	4.88
13-Jan-21	6.73	7.79	1749.8	2025.4	4.69	4.05

productive years of the equipment are represented by i (%) and n, respectively. The annual salvage values is abbreviated as (ASV). For analysis, 260 clear sky days were assumed. The bank's lending interest rate, i was estimated at 15% for funding. The system's estimated life expectancy in several years n, was assumed to be 12 years. Results tabulated in Table 5 show that the lowest CPL values were R4.69 and R4.05 for the MSS-SS and the MSS-SS + BSS, respectively.

$$\mathrm{CRF} = \frac{i(1+i)^n}{\left[(1+i)^n - 1\right]}, \tag{1}$$

$$\mathrm{FAC} = P \times \mathrm{CRF}, \tag{2}$$

$$\mathrm{SFF} = \frac{i}{\left[(1+i)^n - 1\right]}, \tag{3}$$

$$\mathrm{ASV} = \mathrm{SFF} \times S, \tag{4}$$

$$\mathrm{AC} = \mathrm{FAC} + \mathrm{AMC} - \mathrm{ASV}, \tag{5}$$

$$\mathrm{AMC} = 0.15 \times \mathrm{FAC}, \tag{6}$$

$$S = 0.2P, \tag{7}$$

$$\mathrm{CPL} = \frac{\mathrm{AC}}{M}. \tag{8}$$

7. Conclusion

This work reported on the year-round productivity of the vapour-based MSS-SS. The analysis was carried out under three categories of daily average solar radiation, namely, low, moderate, and high. A maximum of 1190 ml distillate was produced under the low range, and the system was least productive due to the low heat input rate. On transitioning from low to moderate range, there was a significant increase in the distillate yield to 6090 ml which was the maximum for the moderate range, suggesting optimum operating conditions for the MSS-SS. However, the removal of the thermal insulation material was necessitated by thermal damage conditions at the upper values of this range. At the high range, there was a marginal increase in daily cumulative distillate yield caused by insufficient vapour cooling and condensation in the condensing tower due to the low thermal inertia of water mass thus, rendering the distillate yield trends to be the inverse of the stages' SW temperature. The maximum distillate yield was 7790 ml at a high daily average range of solar radiation and a 21.8% decrease to 6090 ml on the transition from the high to the moderate range.

A further decline of 80.5% on transitioning from the moderate to the low range. The low thermal inertia of water mass contributed to rapid SW heating and cooling, translating to the maximum vapour production and rapid decline in the desalination process during off-sunshine hours, respectively. The condensing tower necessitated the incorporation of the TES, as the experimental tests revealed that the system had a higher CBA ratio.

8. Future Work

(i) A study on the distillate yield patterns in the stages may yield useful insight in terms of enhancing distillate productivity.

(ii) A considerable increase in the quantity of SW in the zig-zagged tube would eliminate thermal damage conditions and reduce the CBA ratio.

(iii) An optimisation study will account for heat losses in each stage and model heat and mass transfer. Incorporation of AI in the optimisation study to predict the solar still performance may be beneficial. For practical reasons, a considerable improvement in the device efficiency and productivity is required.

(iv) A reduction in vapour make-up tube height (vertical length) could reduce the desalination delays, especially under low rates and impulsive modes of thermal energy inputs.

Abbreviations

AC: Annual cost
AMC: Annual maintenance cost
ASV: Annual salvage value
BSS: Basin solar till
CBA: Collector to basin
CPL: Cost per litre
CRF: Capital recovery factor
CS: Conventional soar still
ETSC: Evacuated tube solar collector
FAC: Fixed annual cost
FBLS: Finned basin liner still
FPSC: Flat plate solar collector
NM: Nonmeasurable
MSS-SS: Multistage solar still with stacked stages
P: Present capital cost
SSF: Sinking fund factor
SW: Saline water
i: Interest per year
n: Number of life years.

Data Availability

The data used in producing this article are available on request.

Conflicts of Interest

The authors declare that they have no conflicts of interest.

Acknowledgments

The authors would like to thank the National Research Foundation for its financial support (grant no. 121389).

References

[1] A. E. Kabeel and S. A. El-Agouz, "Review of researches and developments on solar stills," *Desalination*, vol. 276, no. 1-3, pp. 1–12, 2011.
[2] A. Saxena, E. Cuce, A. E. Kabeel, M. Abdelgaied, and V. Goel, "A thermodynamic review on solar stills," *Solar Energy*, vol. 237, pp. 377–413, 2022.
[3] A. G. Ibrahim and S. E. Elshamarka, "Performance study of a modified basin type solar still," *Solar Energy*, vol. 118, pp. 397–409, 2015.
[4] A. E. Kabeel, T. Arunkumar, D. C. Denkenberger, and R. Sathyamurthy, "Performance enhancement of solar still through efficient heat exchange mechanism–a review," *Applied Thermal Engineering*, vol. 114, pp. 815–836, 2017.
[5] A. O. Alsaiari, S. Shanmugan, H. Abulkhair et al., "Applications of TiO2/Jackfruit peel nanocomposites in solar still: experimental analysis and performance evaluation," *Case Studies in Thermal Engineering*, vol. 38, Article ID 102292, 2022.
[6] A. H. Elsheikh, H. N. Panchal, S. Sengottain, N. A Alsaleh, M. Ahmadein, and M. Ahmadein, "Applications of heat exchanger in solar desalination: current issues and future challenges," *Water*, vol. 14, no. 6, Article ID 14060, 2022.
[7] A. A. El-Sebaii and M. El-Naggar, "Year-round performance and cost analysis of a finned single basin solar still," *Applied Thermal Engineering*, vol. 110, pp. 787–794, 2017.
[8] P. K. Srivastava and S. K. Agrawal, "Winter and summer performance of single sloped basin type solar still integrated with extended porous fins," *Desalination*, vol. 319, pp. 73–78, 2013.
[9] A. F. Muftah, K. Sopian, and M. A. Alghoul, "Performance of basin type stepped solar still enhanced with superior design concepts," *Desalination*, vol. 435, pp. 198–209, 2018.
[10] S. Kumar, G. N. Tiwari, and H. N. Singh, "Annual performance of an active solar distillation system," *Desalination*, vol. 127, no. 1, pp. 79–88, 2000.
[11] A. H. Elsheikh, S. W. Sharshir, M. K. Ahmed Ali et al., "Thin film technology for solar steam generation: a new dawn," *Solar Energy*, vol. 177, pp. 561–575, 2019.
[12] P. V. Kumar, A. K. Kaviti, O. Prakash, and K. S. Reddy, "Optimization of design and operating parameters on the year round performance of a multi-stage evacuated solar desalination system using transient mathematical analysis," *International Journal of Energy and Environment*, vol. 3, no. 3, pp. 409–434, 2012.
[13] A. H. Elsheikh, S. W. Sharshir, M. Abd Elaziz, A. E. Kabeel, W. Guilan, and Z. Haiou, "Modeling of solar energy systems using artificial neural network: a comprehensive review," *Solar Energy*, vol. 180, pp. 622–639, 2019.
[14] A. H. Elsheikh, E. M. El-Said, M. Abd Elaziz, M. Fujii, and H. R. El-Tahan, "Water distillation tower: experimental investigation, economic assessment, and performance prediction using optimized machine-learning model," *Journal of Cleaner Production*, vol. 388, Article ID 135896, 2023.
[15] A. O. Alsaiari, E. B. Moustafa, H. Alhumade, H. Abulkhair, and A. Elsheikh, "A coupled artificial neural network with artificial rabbits optimizer for predicting water productivity of different designs of solar stills," *Advances in Engineering Software*, vol. 175, Article ID 103315, 2023.
[16] M. Feilizadeh, M. Karimi Estahbanati, K. Jafarpur, R. Roostaazad, M. Feilizadeh, and H. Taghvaei, "Year-round outdoor experiments on a multi-stage active solar still with different numbers of solar collectors," *Applied Energy*, vol. 152, pp. 39–46, 2015.
[17] A. K. Tiwari and G. N. Tiwari, "Annual performance analysis and thermal modelling of passive solar still for different inclinations of condensing cover," *International Journal of Energy Research*, vol. 31, no. 14, pp. 1358–1382, 2007.
[18] G. N. Tiwari, J. M. Thomas, and E. Khan, "Optimisation of glass cover inclination for maximum yield in a solar still," *Heat Recovery Systems and CHP*, vol. 14, no. 4, pp. 447–455, 1994.
[19] M. M. Mkhize and V. Msomi, "A comparative study of the multistage solar stills with stacked stages (MSS-SS)," *Journal of Engineering*, vol. 2021, Article ID 7751442, 13 pages, 2021.
[20] Y. Cengel and J. Cimbala, *EBOOK: Fluid Mechanics Fundamentals and Applications (SI Units)*, McGraw Hill, Irvine, CA, USA, 2013.
[21] M. Feilizadeh, M. Karimi Estahbanati, A. S. Ardekani, S. M. E. Zakeri, and K. Jafarpur, "Effects of amount and mode of input energy on the performance of a multi-stage solar still: an experimental study," *Desalination*, vol. 375, pp. 108–115, 2015.
[22] Y. Cengel, J. Cimbala, and R. Turner, *EBOOK: Fundamentals of Thermal-Fluid Sciences (SI Units)*, McGraw Hill, Irvine, CA, USA, 2012.

[23] M. I. Shatat and K. Mahkamov, "Determination of rational design parameters of a multi-stage solar water desalination still using transient mathematical modelling," *Renewable Energy*, vol. 35, no. 1, pp. 52–61, 2010.

[24] E. El-Bialy, S. M. Shalaby, A. E. Kabeel, and A. M. Fathy, "Cost analysis for several solar desalination systems," *Desalination*, vol. 384, pp. 12–30, 2016.

[25] H. E. Fath, M. El-Samanoudy, K. Fahmy, and A. Hassabou, "Thermal-economic analysis and comparison between pyramid-shaped and single-slope solar still configurations," *Desalination*, vol. 159, no. 1, pp. 69–79, 2003.

[26] R. S. Adhikari, A. Kumar, and H. P. Garg, "Techno-economic analysis of a multi-stage stacked tray (MSST) solar still," *Desalination*, vol. 127, no. 1, pp. 19–26, 2000.